Polymer induced drag reduction in exact coherent structures of plane Poiseuille flow

Wei Li and Michael D. Graham[a)]
Department of Chemical and Biological Engineering, University of Wisconsin-Madison, Madison, Wisconsin 53706-1691, USA

(Received 1 November 2006; accepted 3 May 2007; published online 15 August 2007)

Nonlinear traveling waves that are precursors to laminar-turbulent transition and capture the main structures of the turbulent buffer layer have recently been found to exist in all the canonical parallel flow geometries. The present work examines the effect of polymer additives on these "exact coherent states" (ECS) in the plane Poiseuille geometry, using the FENE-P constitutive model for polymer solutions. In experiments with a given fluid, Reynolds and Weissenberg numbers are linearly related (i.e., Wi/Re=const). In this situation, we study the effects of viscoelasticity on velocity field and polymer stress field along some experimental paths, which represent different flow behaviors as Re (and Wi) increases. The changes to the velocity field for the viscoelastic nonlinear traveling waves qualitatively capture many of those experimentally observed in fully turbulent flows of polymer solutions at low to moderate levels of drag reduction: drag is reduced, streamwise velocity fluctuations increase, and wall-normal and spanwise velocity fluctuations decrease. The mechanism underlying these observations is the suppression of streamwise vortices by the polymer forces exerted on the fluid. Specifically, at sufficiently high wall shear rates, viscoelasticity completely suppresses these streamwise vortices in the near-wall region, as is found in experiments in the maximum drag reduction regime. The mean shear stress balance for the nonlinear traveling waves shows that Reynolds shear stress decreases and polymer stress increases monotonically with the increase of viscoelasticity, as is found in full turbulence. The study of the influence of the viscoelasticity on the turbulent kinetic energy and Reynolds stress budgets shows that as Re (and Wi) increases, there is a consistent decrease in the production, diffusion, and dissipation of turbulent kinetic energy. The decrease in the velocity pressure gradient term leads to a redistribution of the turbulent kinetic energy among the streamwise, wall-normal and spanwise directions. The influence of the rheological parameters on the viscoelastic ECS is analyzed. It is found that the degree of drag reduction is determined primarily by the extensional viscosity and Weissenberg number. The optimum wavelength conditions under which the viscoelastic ECS first come into existence are also investigated. The wavelengths in streamwise and spanwise directions and the wall-normal extent of the ECS all increase monotonically with the increase of viscoelasticity, as is found in experiments. © *2007 American Institute of Physics*. [DOI: 10.1063/1.2748443]

I. INTRODUCTION

The reduction of turbulent drag by polymer additives has received much attention since it was first observed experimentally in 1940s that very small polymer concentrations, on the order of ten parts per million by weight, can lead to drag reduction of 50% or greater.[1–4] After six decades of research, the subject remains an active area of research, in part because of applications but also because it lies at the intersection of two complex and important fields: turbulence and rheology. A better understanding of this phenomenon may in turn yield insights into both the dynamics of drag-reducing fluids and of turbulent flows. The goal of the present work is to address turbulent drag reduction in the context of the dominant structures in the turbulent buffer layer, an approach that turns out to touch on many key aspects of the drag reduction phenomenon.

[a)]Author to whom correspondence should be addressed. Electronic mail: graham@engr.wisc.edu

Studies of drag-reducing fluids indicate that at least near on onset Reynolds number for drag reduction, the effects of the polymer are confined primarily to the buffer layer region of the flow,[1,5–8] where the production and dissipation of turbulent kinetic energy peak.[9] Experimental observations and direct numerical simulation (DNS) studies show that the dominant structures of the buffer layer are pairs of streamwise-aligned, counter-rotating vortices.[9–11] These vortices pull slower moving fluid away from the wall, forming low-speed, streamwise velocity streaks. In drag-reducing flows, these structures are modified by polymers: the buffer region thickens,[1] the coherent structures in this region shift to larger scales,[5,12–14] and the bursting rate decreases.[5] These structural changes are accompanied by enhanced root-mean-square (rms) streamwise velocity fluctuations (at least in the moderate drag reduction region) and reduced rms wall-normal and spanwise velocity fluctuations.[15] Moreover, streamwise vorticity fluctuations[12] and Reynolds shear stress[12,16,17] are also decreased. These changes become more pronounced as the extensional viscosity of the polymer solu-

tion is increased.[8,16,18,19] More recent experimental results[20,21] reveal that in the maximum drag reduction (MDR) region the ejections from the wall are eliminated and the wall vortices that sustain turbulence in a Newtonian fluid are completely destroyed. Low-speed streamwise velocity streaks are essentially absent. A recent DNS study[22] also shows that in this regime the streamwise-aligned vortices are greatly or almost entirely suppressed, while the number of hairpin type vortices is increased. These observations suggest that the coherent structures in buffer layer region are crucial in addressing rheological drag reduction in wall-bounded turbulent flows.

To better understand the effect of polymer on the buffer layer, we wish to study a model flow that has similar structures as seen in this region but without the full complexities of time-dependent turbulent flow. A recent advance in this direction has come with the recognition that the Navier-Stokes equations support nonlinear traveling wave states, the family of so-called "exact coherent states" (ECS). These states capture the dominant streamwise-aligned counter-rotating vortex pairs that flank streaks in the streamwise velocity. These states have been found in plane Couette flow,[23–26] plane Poiseuille flow[27–29] and pipe flow.[30,31]

We focus here on the plane Poiseuille geometry (pressure-driven channel flow) with average wall shear stress τ_w, of a fluid with dynamic viscosity η, density ρ, and kinematic viscosity $\nu=\eta/\rho$. The centerline laminar velocity U and half-channel height l define outer scales for the flow. Inner scales are the friction velocity $u_\tau=\sqrt{\tau_w/\rho}$ and the near-wall length scale $l_w=\nu/u_\tau$. As usual, quantities expressed in terms of these so-called "wall units" are denoted with a superscript "+." The friction Reynolds number $\mathrm{Re}_\tau=u_\tau l/\nu$ is simply the half-channel height expressed in wall units. The Weissenberg number is denoted $\mathrm{Wi}=\lambda\dot{\gamma}_w=\lambda u_\tau^2/\nu$, where λ is polymer relaxation time and $\dot{\gamma}_w$ is the average wall shear rate. Experimental results for a given fluid and flow geometry lie on curves of constant elasticity parameter $\mathrm{El}=2\lambda\nu/l^2$.

Figure 1 shows the streamwise velocity field and the streamwise vortices for one of these states at the minimum Reynolds number at which the ECS can exist for Newtonian flow. Note that there is no turbulent core in the channel. The channel is composed of two buffer layer regions with one sitting on top of the other; reflection symmetry boundary conditions (as discussed in Sec. II) are imposed at the channel centerline. The streamwise vortices are identified using the Q-criterion as discussed in Refs. 32–34. The isosurfaces of Q isolate areas where the strength of rotation overcomes the strain. In our study, we use a two-dimensional (2D) Q-criterion to eliminate the strong effect of the shear at the wall: $Q=\frac{1}{2}(\|\mathbf{\Omega}_{2D}\|^2-\|\mathbf{D}_{2D}\|^2)$, where $\mathbf{\Omega}_{2D}=\frac{1}{2}(\nabla\mathbf{v}_{2D}-\{\nabla\mathbf{v}_{2D}\}^T)$ and $\mathbf{D}_{2D}=\frac{1}{2}(\nabla\mathbf{v}_{2D}+\{\nabla\mathbf{v}_{2D}\}^T)$ are vorticity tensor and rate of strain tensor, respectively; $\nabla\mathbf{v}_{2D}=(\partial v_y/\partial y,\ \partial v_z/\partial y;\ \partial v_y/\partial z,\ \partial v_z/\partial z)$. The ECS are periodic in the streamwise (x) and spanwise (z) directions; for a given pair of wavelengths (L_x,L_z), they appear in pairs at finite amplitude in saddle-node bifurcations as the Reynolds number Re increases. While both of these solutions are unstable, one of these states, which we will call the "high drag" state

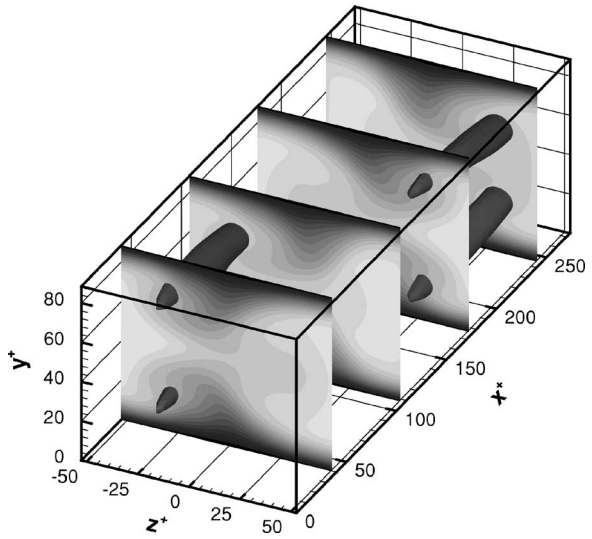

FIG. 1. A nonlinear traveling wave state at Re=977 (Re_τ=44.2) in the plane Poiseuille geometry. The full channel is shown, with the two walls located at $y^+=0$ and 88.4, respectively. The panels show contours of streamwise velocity v_x (white for the highest velocity, black for the lowest velocity). The constant isosurfaces are $Q^+=0.008$ (black).

due to its lower mean velocity at a given Reynolds number, has greater stability relative to the "low drag" ECS—the high drag solutions have one more stable direction in phase space than the low drag solutions. Recently, Waleffe and Wang have shown that these states are unconnected with the laminar state even as the Reynolds number tends to infinity.[35] For Couette flow with no-slip boundary conditions, the ECS first appear at $\mathrm{Re}\approx 128$ (see Ref. 29) (i.e., this Reynolds number is the lowest for which an ECS solution can be found for any wavelength pair), where the Reynolds number is based on half the velocity difference between the walls and the half-channel height. For pipe flow, they appear at $\mathrm{Re}\approx 1300$,[30] where the Reynolds number is based on the laminar centerline velocity and pipe radius, and in the case of interest here, i.e., plane Poiseuille flow, they appear at Re=977, where the Reynolds number is based on the laminar centerline velocity and the half-channel height. The appearance of the ECS presages the transition to turbulence in all these geometries. In Couette flow, persistent turbulence is seen for $\mathrm{Re}\gtrsim 325$,[36] for pipe flow at $\mathrm{Re}\gtrsim 2100$,[37] and for channel flow at $\mathrm{Re}\gtrsim 1000$.[38] Note that these experimental values for transition are for the existence of persistent, fully developed turbulence; intermittent turbulent spots can appear well below these values.

The connection between ECS in plane Poiseuille flow and near-wall turbulence can be further supported by a study of length scales.[29] The friction Reynolds number Re_τ $(=\sqrt{2\mathrm{Re}})$ at which the plane Poiseuille flow ECS appear is 44.2. This is simply the wall-normal extent of the ECS, expressed in wall units. The spanwise wavelength $L_z^+=105.6$ of the ECS at onset closely captures the streak spacing of $\sim$100 wall-units widely observed in experiments over a large range of Reynolds numbers.[9] Minimal channel flow, i.e., flow in the smallest computational domain that reproduces the velocity field statistics of near-wall turbulence,

gives a range for the streamwise length L_x^+ of 250–350, compared to $L_x^+=273.7$ for the ECS, and a spanwise length that is again approximately 100 wall units.[39] In the minimal channel flow the statistics of the near-wall region are faithfully captured up to a wall-normal distance $y^+\approx 40$, while again we note that the wall-normal size of the onset ECS is $L_y^+=\mathrm{Re}_\tau=44.2$. It should be pointed out that this minimum channel contains a single wavelength of a wavy streak and a pair of quasi-streamwise vortices, which is the same structure seen in the ECS. Another approximately Reynolds-number-invariant length scale in near-wall turbulence is the peak in the production of turbulent kinetic energy at $y^+\approx 12$;[40] the channel flow ECS also captures this length scale.[41] The length scales at which the ECS first appear are in close agreement with the length scales of near-wall turbulence.

Beyond capturing the observed length scales of the buffer region structures, recent research also indicates that the ECS are saddle-points in phase space around which the strange attractor[42] of near-wall turbulence is built. Recent studies by Kawahara and Kida[43] and Toh and Itano[44] find periodic solutions in minimal channel flows that are bifurcations of the ECS. The bursting trajectories in fully turbulent flows seem to be built around these periodic solutions. A further indication of this comes from a study by Jiménez and Simens that applies a numerical filter to DNS of channel flow to isolate the near-wall region from the mainstream turbulence.[45] The simplest (nontrivial) flow structure, found when the numerical mask is at $y^+\approx 50$, is a traveling-wave solution that has qualitatively the same structure as the ECS. The length scales of this traveling wave ($L_x^+\approx 250$, $L_y^+\approx 50$, and $L_z^+\approx 150$) are similar to the optimum values for the channel flow ECS described above. As the mask moves further away from the wall, these traveling-wave solutions bifurcate into quasiperiodic solutions. These solutions then evolve into bursts of full-scale turbulence with the flow being essentially turbulent when the numerical filter reaches $y^+\approx 70$. These results along with the existence of the ECS indicate that staggered streamwise vortex traveling wave patterns are autonomous in wall-bounded shear flows and provide, at least in part, the foundation on which the near-wall turbulent fluctuations are built.

The self-sustaining process that underlies the ECS consists of three interacting, concurrent subprocesses: (1) a perturbation of the base flow in the form of weak streamwise vorticities redistributes the streamwise momentum to create large spanwise fluctuations in the streamwise velocity, i.e., the "streak"; (2) the spanwise inflections lead to three-dimensional Kelvin-Helmholtz-like instability in which a three-dimensional disturbance develops; (3) the concentrated vorticity arising from the instability develops into almost streamwise-staggered vortices that regenerate the streaks.[46–48]

Because the first effects of the polymer arise in the buffer region, whose structures the ECS evidently capture, these flows provide a natural starting point for understanding drag reduction. In prior work, we have studied the initial effects of viscoelasticity on ECS in the plane Couette and plane Poiseuille geometries.[49–52] Those studies provided some structural insight into the mechanism of drag reduction. The polymer molecules become highly elongated as they move through the streamwise streak. As they move out of the streak and into one of the vortices, the polymer molecules relax. This relaxation produces a polymer force that reduces the strength of the vortices, which causes the self-sustaining process to collapse and leads to drag reduction, as is found by DNS studies.[53] In our recent work, we have taken a broader view, examining the region of parameter space (Re, Wi) in which ECS exist and its connection to experimental observations.[54] A schematic is proposed, which captures many key aspects of turbulent drag reduction, including the delay in transition to turbulence, drag reduction onset thresholds, and diameter and concentration effects. At sufficiently high wall shear rates, viscoelasticity is found to completely suppress these ECS, as is found in recent experimental and DNS studies in the MDR region.[20–22]

The present work addresses the effect of viscoelasticity on exact coherent states in the plane Poiseuille geometry. We illustrate the changes in the bifurcation diagram and the corresponding changes in the region of parameter space in which these solutions exist. In particular, the changes in the velocity field and polymer stress field along some experimental paths are studied. These results are then related to the physics of the interaction between the polymer dynamics and the flow field, to illustrate the physical mechanism by which viscoelasticity affects these states. These changes are further investigated through budgets of turbulent kinetic energy, Reynolds stress and mean shear stress. The influence of rheological parameters on viscoelastic ECS and the changes in optimum wavelengths of viscoelastic ECS are also studied.

II. MATHEMATICAL FORMULATION AND SIMULATION DETAILS

Denoting the streamwise direction as x, the wall-normal direction as y, and the spanwise direction as z, we consider pressure-driven flow with no-slip boundary conditions at the wall

$$v_x = v_y = v_z = 0 \quad \text{at } y = -1, \tag{1}$$

where v_x, v_y, and v_z are streamwise, wall-normal, and spanwise components of the velocity $\mathbf{v}$, respectively. We will only simulate half of the channel and apply reflection symmetry boundary conditions at the channel centerline $y=0$:

$$\frac{\partial v_x}{\partial y} = v_y = \frac{\partial v_z}{\partial y} = 0. \tag{2}$$

The laminar centerline velocity U and the half-channel height l are used to scale velocity and position, respectively. Time t is scaled with l/U, and pressure p with ρU^2. The stress due to the polymer, i.e., $\boldsymbol{\tau}_p$, is nondimensionalized with the polymer elastic modulus $G=\eta_p/\lambda$, where η_p is the polymer contribution to the viscosity and λ is the time constant for the polymer—the polymer model is described below. The momentum balance and the equation of continuity are

$$\frac{\partial \mathbf{v}}{\partial t} + \mathbf{v}\cdot\nabla\mathbf{v} = -\nabla p + \beta\frac{1}{\mathrm{Re}}\nabla^2\mathbf{v} + (1-\beta)\frac{2}{\mathrm{Re\,Wi}}(\nabla\cdot\boldsymbol{\tau}_p), \tag{3}$$

$$\nabla \cdot \mathbf{v} = 0, \tag{4}$$

where η_s is the solvent viscosity, $\mathrm{Wi} = \lambda \dot{\gamma}_w$ is the Weissenberg number based on wall shear rate, $\dot{\gamma}_w = 2U/l$, and $\beta = \eta_s/(\eta_s + \eta_p)$ is the fraction of the total zero-shear viscosity that is due to the solvent. The Reynolds number Re is based on the total viscosity: $\mathrm{Re} = \rho U l/(\eta_s + \eta_p)$. This paper is concerned with traveling wave solutions of the form $\mathbf{v}(x,y,z,t) = \mathbf{v}(x - Ct, y, z, 0)$, where the traveling wave velocity C is part of the solution. Looking for such solutions is equivalent to looking for a three-dimensional velocity field $\mathbf{v}(x,y,z)$ that satisfies the above mentioned equations with ∂_t replaced by $-C\partial_x$. We seek "sinuous" traveling wave solutions that satisfy the shift-reflect symmetry

$$v_x(x,y,z) = v_x(x + L_x/2, y, -z), \tag{5}$$

$$v_y(x,y,z) = v_y(x + L_x/2, y, -z), \tag{6}$$

$$v_z(x,y,z) = -v_z(x + L_x/2, y, -z). \tag{7}$$

The polymer stress is computed with the FENE-P constitutive model, in which each polymer molecule consists of two beads, where the mass and drag of the molecule are concentrated, connected by a FENE (finitely extensible nonlinearly elastic) spring. The governing equation for this model is[55]

$$\frac{\boldsymbol{\alpha}}{1 - (\mathrm{tr}\,\boldsymbol{\alpha}/b)} + \frac{\mathrm{Wi}}{2}\left(\frac{\partial \boldsymbol{\alpha}}{\partial t} + (\mathbf{v}\cdot\nabla\boldsymbol{\alpha}) - \{\boldsymbol{\alpha}\cdot\nabla\mathbf{v}\} - \{\boldsymbol{\alpha}\cdot\nabla\mathbf{v}\}^T\right) = \left(\frac{b}{b+2}\right)\boldsymbol{\delta}, \tag{8}$$

where $\boldsymbol{\alpha}$ is a nondimensional conformation tensor and b is proportional to the maximum extension of the dumbbell—$\mathrm{tr}\,\boldsymbol{\alpha}$ cannot exceed b. The polymer contribution to the stress is given by

$$\boldsymbol{\tau}_p = \frac{b+5}{b}\left[\frac{\boldsymbol{\alpha}}{1 - (\mathrm{tr}\,\boldsymbol{\alpha}/b)} - \left(1 - \frac{2}{b+2}\right)\boldsymbol{\delta}\right]. \tag{9}$$

It is well recognized that extensional rheology plays a key role in turbulent drag reduction. A simple measure of the importance of extensional polymer stress is the relative magnitude of the polymer and solvent contributions to the steady state extensional stress in uniaxial extension. We define the extensibility parameter

$$\mathrm{Ex} \equiv \frac{\eta_\infty^+}{3\eta_s}, \tag{10}$$

where η_∞^+ is the polymer contribution to the steady state uniaxial extensional viscosity of the fluid in the limit of high extension rate. For the FENE-P model this expression becomes

$$\mathrm{Ex} = \frac{2b(1-\beta)}{3\beta}. \tag{11}$$

We consider the situation $1 - \beta \ll 1$, in which case shear-thinning is negligible, as the polymer contributes only a very small amount to the total shear viscosity of the solution. In this situation, significant effects of the polymer on the flow are expected only when $\mathrm{Ex} \gg 1$. Finally, note that experimental results for a given fluid and flow geometry lie on curves of constant elasticity parameter $\mathrm{El} = 2\lambda(\eta_s + \eta_p)/\rho l^2 = \mathrm{Wi}/\mathrm{Re}$. For this reason, we will call lines with constant El "experimental paths."

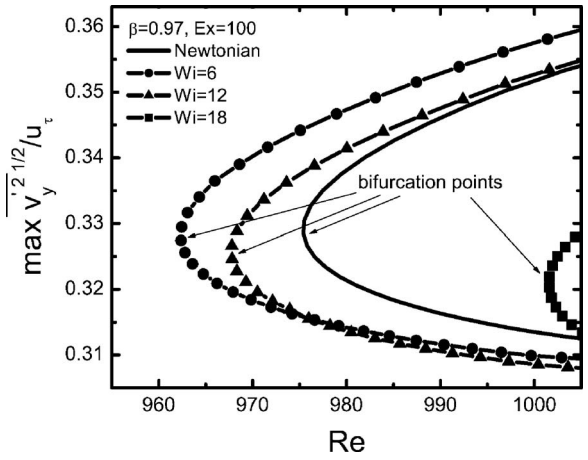

FIG. 2. Bifurcation diagram for Newtonian and viscoelastic ECS; $L_x = 2\pi/1.0148$ and $L_z = 2\pi/2.633$ (Ref. 54).

The conservation and constitutive equations are solved through a Picard iteration. A Newtonian ECS, as computed in Ref. 27, is first used to calculate the polymer stress tensor $\boldsymbol{\tau}_p$ by inserting the velocity field in the evolution equation for $\boldsymbol{\alpha}$ and integrating for a short length of time, usually one time unit (l/U). For this $\boldsymbol{\tau}_p$, a steady state of the momentum and continuity equations is found by Newton iteration. The resulting velocity field $\mathbf{v}$ is used to compute the new $\boldsymbol{\tau}_p$, and the process is repeated until the velocity and polymer field converge to a steady state.

The momentum and continuity equations are discretized using a Fourier-Chebyshev formulation with typically a $9 \times 17 \times 9$ grid. The conformation tensor $\boldsymbol{\alpha}$ is discretized with a third-order, compact upwind difference scheme.[56,57] In this, as in most previous computational studies of polymers in turbulent flows, we have found it necessary to add an artificial stress diffusivity $[(1/(\mathrm{Sc}\,\mathrm{Re})]\nabla^2\boldsymbol{\alpha}$, to Eq. (8) to achieve numerical stability. The Schmidt number Sc, which is the ratio of the momentum diffusivity to stress diffusivity, is set to value of 1.0. This value of Sc, though artificially small, is greater than or of the same order of magnitude as that used in many DNS studies.[12,17,58,59] In the range of Sc where solutions can be obtained, the bifurcation diagrams shown in Fig. 2 are insensitive to its value. The stress diffusion term is integrated implicitly by the Crank-Nicholson method with the other terms of the equation integrated using the Adams-Bashforth method. This equation is solved on a finer mesh than the momentum, continuity pair—typically $48 \times 49 \times 48$. Higher resolutions ($10 \times 19 \times 10$ for the momentum, continuity pair, and $64 \times 65 \times 64$ for the polymer stress) show less than a 0.35% change in the centerline mean streamwise velocity $U_{\max}$ at $\mathrm{Re} = 1600$ and $\mathrm{Wi} = 32$ compared to the lower resolutions.

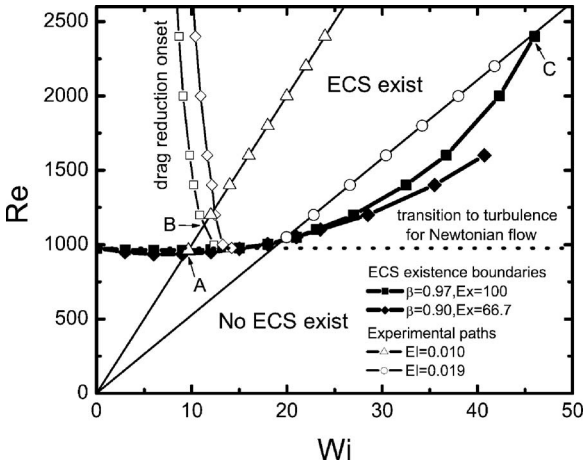

FIG. 3. Existence boundaries and drag reduction regimes for viscoelastic ECS; $L_x=2\pi/1.0148$ and $L_z=2\pi/2.633$ (Ref. 54).

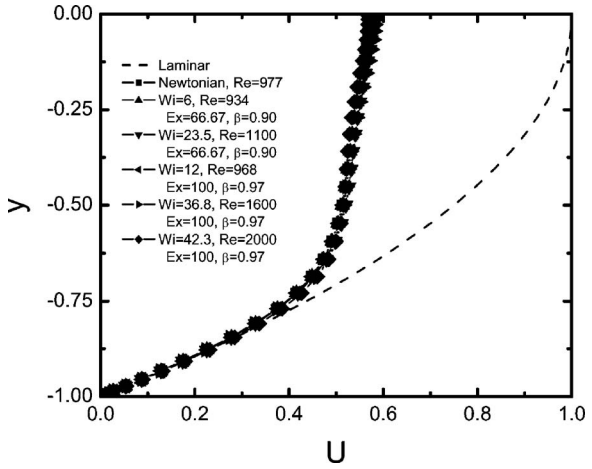

FIG. 4. Mean streamwise velocity for Newtonian and viscoelastic ECS on the ECS existence curve; $\beta=0.97$, Ex=100 (Ref. 54).

III. RESULTS

A. Existence of the ECS

In the Newtonian limit, the minimum Reynolds number at which ECS exist is Re=977 ($\mathrm{Re}_\tau=44.2$), with $L_x=2\pi/1.0148$ and $L_z=2\pi/2.633$. All results presented in this section are with these "optimal" length scales. (The effects of viscoelasticity on the optimal length scales will be discussed in the later part of this paper.) In inner units, these lengths correspond at $\mathrm{Re}_\tau=44.2$ to $L_x^+=273.7$ and $L_z^+=105.5$. These states arise via a saddle-node bifurcation as shown in Fig. 2. The solutions are plotted using the maximum in the root mean square wall-normal velocity fluctuations for the solution $(\overline{v_y'^2})^{1/2}$. (Hereafter, an overbar indicates that the variable is averaged over the streamwise and spanwise directions.) The solutions with higher maximum wall-normal velocity at a given Re are called "high drag" solutions due to their lower mean velocity at the centerline of the channel compared to the "low drag" solutions. All results in this paper are for the high drag states. Although both solutions are unstable, their status as precursors to transition and their structural similarity to buffer layer turbulence suggest that they are saddle points that underlie in part the strange attractor of turbulent flow.

Figure 2 indicates that the addition of polymer changes the Reynolds number $\mathrm{Re}_{\min}$ at which the ECS come into existence (i.e., the position of the saddle-node bifurcation points). Curves of ECS existence boundaries $\mathrm{Re}_{\min}$ versus Wi are given, for two parameter sets, by the thick solid curves on Fig. 3. These separate the region where the ECS can exist (above the curves) from the region where no ECS exist, for the given values of Ex and β. With our current computational approach, the highest Re and Wi that are accessible for Ex=100 and $\beta=0.97$ are about 2500 and 46, respectively. However, higher Re and Wi may be accessible with Newton iteration directly on the entire coupled system of momentum and polymer conformation equations, along with the wave speed parameter.

While at low Wi, there is a slight decrease in $\mathrm{Re}_{\min}$ from the Newtonian value, once Wi exceeds about 45, $\mathrm{Re}_{\min}$ for Ex=100 is more than doubled. This dramatic increase in $\mathrm{Re}_{\min}$ after onset is consistent with the experimental observation that the transition to turbulence in a polymer solution is delayed to higher Re than in the Newtonian case.[8,60,61] Recall that the Reynolds number is simply related to the wall-normal length scale of the structure measured in wall units, i.e., $\mathrm{Re}=(L_y^+)^2/2$ (and in the present situation, $L_y^+=\mathrm{Re}_\tau$). In experiments the thickness of the buffer region (the wall-normal extent of this region in wall units) is known to increase as drag reduction increases.[1] The results for the viscoelastic ECS closely mirror this increase in L_y^+. The curve labeled "drag reduction onset" denotes where the centerline mean velocity $U_{\max}$ of the viscoelastic upper branch ECS first exceeds that of the Newtonian upper branch ECS at the same Reynolds number. This onset Weissenberg number $\mathrm{Wi}_{\mathrm{onset}}$ decreases with increasing Reynolds number; it approaches $\mathrm{Wi}_{\mathrm{onset}}\approx 9$ at $\mathrm{Re}\approx 2400$, which is slightly high compared to the result $\mathrm{Wi}_{\mathrm{onset}}\approx 6$ predicted by two recent viscoelastic DNS studies,[19,62] but in those studies El was significantly smaller, and the onset Reynolds number correspondingly larger, than the values considered here—and in any case there is no reason to expect exact correspondence between onset values from DNS results for fully turbulent flow and the ECS, as the former is more complex than the latter.

Figure 4 shows mean velocity profiles at six different sets of parameter values, each corresponding to a point on the existence boundary for the ECS (i.e., a bifurcation point). Remarkably, when plotted in outer units, they all fall on virtually the same curve. Therefore, at least for the values of Re and Wi that are currently accessible in our simulations, we observe that mean velocity profiles at onset of the ECS have a roughly universal form, which is insensitive to polymer extensibility, concentration, Weissenberg number, or Reynolds number.

We now turn to the study of the evolution of the ECS along some experimental paths; i.e., lines of constant El. Two such paths, denoted by the thin solid lines with hollow symbols, are shown in Fig. 3. Consider first the case El=0.010; as Re and Wi increase, the path intersects the ECS existence

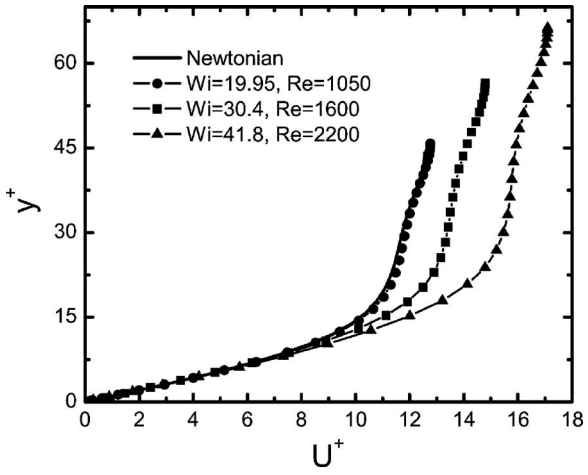

FIG. 5. Mean streamwise velocity for Newtonian and viscoelastic ECS along the experimental path of El=0.019, Ex=100, β=0.97 (Ref. 54). Note that at Re=1050, 1600, and 2200, the channel centerlines are at y^+=45.8, 56.6, and 66.3, respectively.

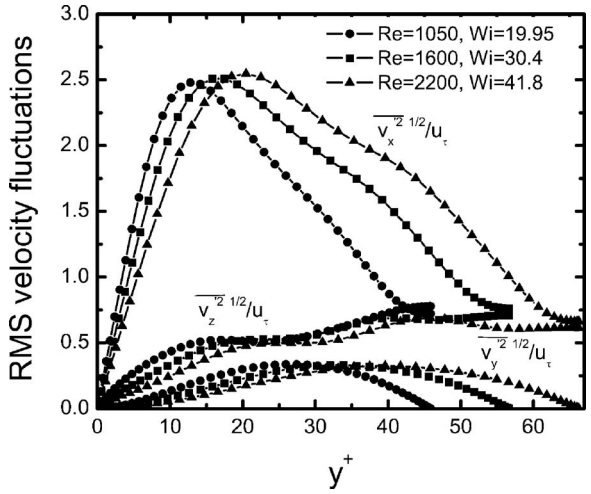

FIG. 6. Fluctuations in the streamwise, wall-normal, and spanwise velocities along the experimental path of El=0.019, Ex=100, β=0.97.

boundary at point *A* and the drag reduction onset threshold curve at point *B*, where the transition to turbulence and the onset of drag reduction occur, respectively. Turning to the case El=0.019, mean velocity profiles expressed in wall units are shown for various values of Re in Fig. 5. For this parameter set, drag reduction is observed immediately upon onset of the ECS. For Re=2200, Wi=41.8, the degree of drag reduction, defined as the percentage decrease in the friction factor relative to that of the Newtonian ECS at the same Re (i.e., wall shear rate), is about 40%.

Continuing upward in Re and Wi at El=0.019, the path re-intersects the ECS existence boundary at point *C* in Fig. 3. (We suspect that this will also happen in the El=0.010 case, but at higher Re and Wi than are accessible with our current computational approach.) Above this point the flow can no longer sustain these ECS; viscoelasticity completely suppresses the near-wall vortical structures. This result is consistent with experimental observations and DNS results in the MDR regime that, at least at relatively low friction Reynolds number, the eruptions of low-momentum fluid from the wall are eliminated and the near-wall streamwise vortices are significantly or almost completely destroyed.[20–22] Note, however, that in the MDR regime the flow does not relaminarize, as would be suggested by a scenario based only on the ECS. Thus, we conjecture that as the ECS are suppressed, other structures are unmasked and in the MDR regime become dominant.

The changes to the average rms streamwise, wall-normal, and spanwise velocity fluctuations along the experimental path of El=0.019, each scaled by the friction velocity u_τ, are given in Fig. 6. The peak in $(\overline{v_x'^2})^{1/2}$ occurs at $y^+ \approx 12$ with peak value of about 2.5, both of which are very close to 12 and 2.7 found in experiments and DNS of fully turbulent flows.[63,64] For the viscoelastic ECS, this peak shifts away from the wall monotonically with the increase of viscoelasticity. Away from the wall, the rms streamwise velocity fluctuations increase significantly with the increase of viscoelasticity while the rms wall-normal and spanwise velocity fluctuations decrease. Note that the ECS have no turbulent core, as shown in Fig. 1. By symmetry, $v_y=0$ at the channel centerline, so $(\overline{v_y'^2})^{1/2}$ vanishes there. Contrarily, DNS of minimal channel flows[39,45] and fully turbulent flows[12,53,62] contain a homogeneous turbulent core at the center of the channel, which produces uniform nonzero rms velocity fluctuations in that region. However, the monotonic increase in $(\overline{v_x'^2})^{1/2}$ and the monotonic decrease in $(\overline{v_y'^2})^{1/2}$ and $(\overline{v_z'^2})^{1/2}$ with the increase of viscoelasticity, as shown in Fig. 6, are consistent with experimental observations and DNS results.[1,12] The viscoelastic effect can also be observed in the reduced Reynolds shear stress $-\rho\overline{v_x'v_y'}$, as shown in Fig. 7. Near the wall, it can be shown (see, e.g., Ref. 40) that the Reynolds shear stress scales as y^{+3}. Near the channel centerline, no such result holds; we do not have a specific explanation as to why the Reynolds shear stress is so small there. The Reynolds shear stress peaks in the buffer layer region with its peak location at $y^+ \approx 30$, which is in good agreement with this peak location at $y^+ \approx 30$ observed in fully turbulent flows.[12,62] For the viscoelastic ECS, this peak shifts away

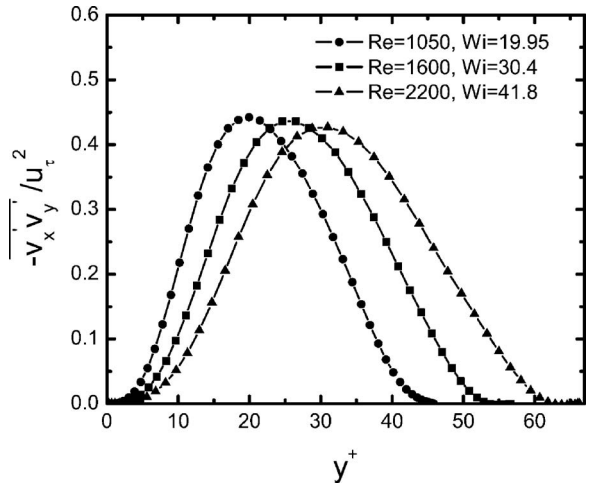

FIG. 7. Reynolds shear stress along the experimental path of El=0.019, Ex=100, β=0.97.

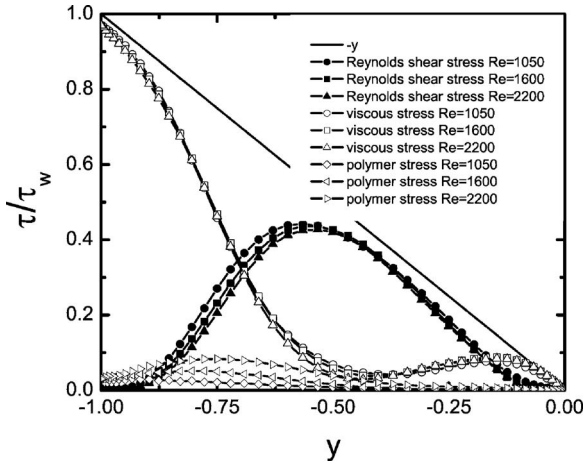

FIG. 8. Stress balance for viscoelastic ECS along El=0.019, Ex=100, β=0.97.

from the wall monotonically with the increase of viscoelasticity, as it does in experiments and DNS of fully turbulent flows.[12,62] The distance of this peak away from the channel centerline is, however, determined by Reynolds number. The ECS results here are at low Reynolds number relative to DNS results. Since the Reynolds shear stress is the wall-normal flux of streamwise momentum, this result provides a further indication of drag reduction in the viscoelastic ECS.

Figure 8 shows the contributions to the mean shear stress as a function of distance from the wall. The stress balance is given by

$$-y = \frac{\beta}{\mathrm{Re}}\frac{1}{u_\tau^2}\frac{dV_x}{dy} - \frac{\overline{v_x'v_y'}}{u_\tau^2} + \frac{2(1-\beta)}{\mathrm{Re\ Wi}}\frac{\overline{\tau_{p_{xy}}}}{u_\tau^2}, \tag{12}$$

where the scaled Reynolds shear stress is $-\overline{v_x'v_y'}/u_\tau^2$, the Newtonian viscous stress is $(\beta/\mathrm{Re})(1/u_\tau^2)(dV_x/dy)$, and the mean polymer stress is $[2(1-\beta)/(\mathrm{Re\ Wi})](\overline{\tau_{pxy}}/u_\tau^2)$. Again we observe qualitative agreement with DNS results.[12,17] Reynolds shear stress for viscoelastic ECS decreases monotonically with the increase of viscoelasticity throughout the whole channel. The average polymer shear stress shows a monotonic increase with the increase of viscoelasticity.

Figure 9 shows the product of velocity fluctuations and the corresponding components of polymer force

$$\mathbf{f} = \frac{2(1-\beta)}{\mathrm{Re\ Wi}}\,\nabla\cdot\boldsymbol{\tau}_p$$

in wall-normal and spanwise directions, along with the isosurfaces of Q^+ (which is used to identify the streamwise vortices). The black regions around the streamwise vortices indicate the anti-correlation between velocity fluctuations and polymer forces, i.e., the regions where the wall-normal velocity is positive are matched by the negative regions of the polymer force and likewise, negative regions of wall-normal velocity correspond to positive polymer force; similar results can also be observed in the spanwise velocity and polymer force. This anti-correlation of polymer force with the fluctuation velocity has also been found in DNS of drag reducing solutions[65] and more recently by Stone *et al.*[51] in plane Couette flow ECS and by Li *et al.*[52,54] in plane Poiseuille flow ECS. Recalling the importance of these streamwise aligned vortices in the self-sustaining process in the redistribution of mean shear, these results indicate that the added polymer stress is working to suppress the mechanism of the ECS.

Further insight into the influence of the polymers on the ECS can be gained by studying the spatial distribution of the polymer stress $\boldsymbol{\tau}_\mathbf{p}$ and the associated streamwise vortices. Figure 10 shows the distribution of tr $\boldsymbol{\tau}_\mathbf{p}$ and isosurfaces of Q^+ in the channel for various values of Re (and Wi) along the experimental path of El=0.019. At relatively low Re (and Wi), polymer molecules are only highly stretched in the near-wall region due to the high shear rate at the wall. As Re (and Wi) increases, the polymer stress is significantly increased in both near the wall region and the upwellings between vortices. Furthermore, we see that highly stretched

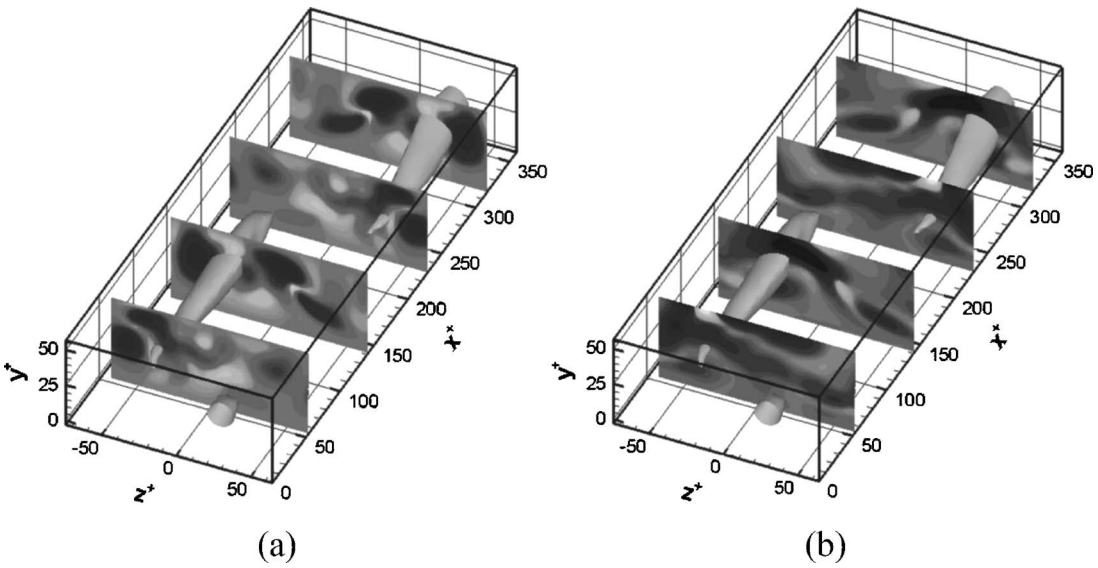

FIG. 9. Products of velocity fluctuations and polymer forces. The constant isosurfaces are Q^+=0.005 75. Re=1600, Wi=30.4, Ex=100, and β=0.97. (a) $v_y f_y$, range -1.0×10^{-4} (black) to 5.9×10^{-6} (white). (b) $v_z f_z$, range -5.3×10^{-4} (black) to 3.3×10^{-4} (white).

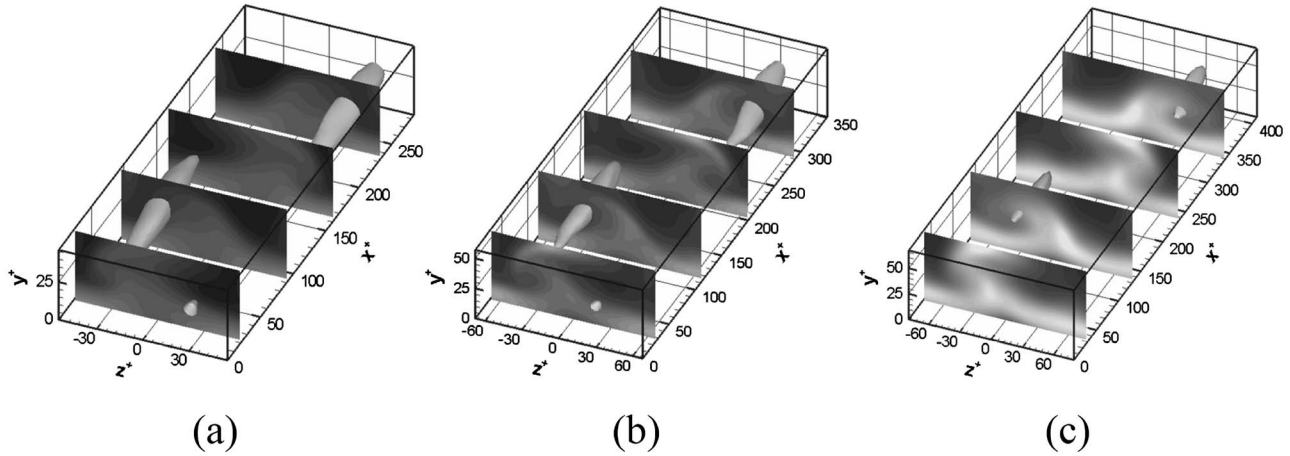

FIG. 10. Trace of the polymer stress along the experimental path of El=0.019, Ex=100, β=0.97, range 0 (black) to 3300 (white). The constant isosurfaces are Q^+=0.008. (a) Re=1050, Wi=19.95; (b) Re=1600, Wi=30.4; (c) Re=2200, Wi=41.8.

molecules are now getting "wrapped into" the streamwise vortices, where they relax—this relaxation generates the polymer forces that reduce the strength of the vortices, which causes the self-sustaining process to collapse and leads to drag reduction. This observation is more evident by looking at the evolution of streamwise vortices along the same experimental path. As Re (and Wi) increases, the isosurfaces of Q^+ become smaller, indicating that the strength of the vortices is diminishing. In Fig. 10(c), the streamwise vortices are almost entirely suppressed by viscoelasticity, which is consistent with the observation that this ECS solution at Re =2200 and Wi=41.8 (the open circle just left of label "C" in Fig. 3) is very close to the ECS existence boundary, below which the streamwise vortices are too weak to sustain these nonlinear traveling waves. Figure 10 shows a significant increase of the trace of polymer stress $\boldsymbol{\tau}_p$ at the centerline region as Re (and Wi) increases. This result indicates that in that region, the polymer molecules are highly stretched in the spanwise direction.

Besides the distribution of polymer stress, polymer dynamics in the plane Poiseuille ECS can be understood by looking at how polymer molecules move through the flow. As stated earlier, the ECS appear as steady solutions in an Eulerian reference frame that moves at the wave speed for the solution. However in a Lagrangian reference frame, i.e., a frame that describes the dynamical history of a selected fluid element,[66] the ECS are chaotic, as we now show. As a first illustration of the qualitative dynamics of fluid trajectories in the ECS flow, we examine a Poincaré map of the flow, constructed by following a fluid element through the flow and marking where it intersects a plane x=const. Since the ECS flow is periodic in the streamwise and spanwise directions, a

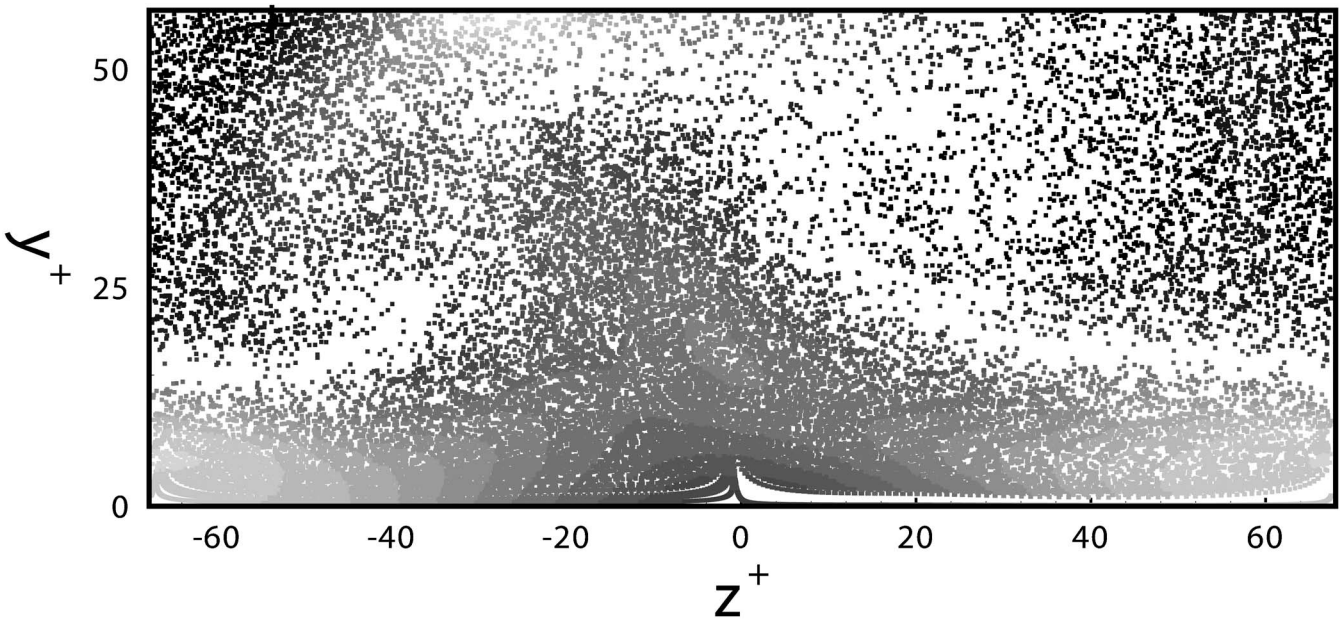

FIG. 11. Poincaré map; x^+=43.8, Re=1600, Wi=30.4, Ex=100, β=0.97. Contours are for trace of the polymer stress, tr $\boldsymbol{\tau}_p$. Range: 0 (black) to 1860 (gray).

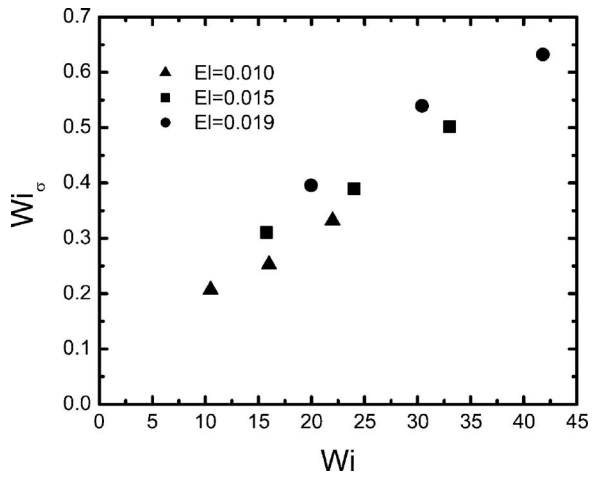

FIG. 12. Changes of Wi_σ as Wi increases; Ex=100, β=0.97.

given trajectory will cross a given plane x=const many times. Figure 11 shows a Poincaré map obtained by marking where the trajectory starting at position x^+=43.8, y^+=56.1, z^+=−53.6 (black "+" in Fig. 11), with Re=1600 and Wi =30.4, intersects the plane x^+=43.8 (moving in the positive x direction at the wave speed for the solution) for up to 10^6 time units. The color coding indicates the magnitude of tr $\boldsymbol{\tau}_\mathbf{p}$ on the trajectory. The single trajectory ultimately samples almost the entire plane, indicating that it is chaotic. We found qualitatively identical results independent of the initial condition or intersection plane chosen.

An important consequence of chaotic flow kinematics for polymer dynamics is that in chaotic flows, material lines stretch exponentially fast. The average line stretching rate, measured along a trajectory, is equivalent to the largest Liapunov exponent, which we denote as $\sigma_{\max}$ (see Ref. 67 for numerical computation of Liapunov exponents). It is straightforward to show (see, e.g., Refs. 50 and 68–71) that, for a Hookean dumbbell model of a polymer ($b\to\infty$), if $\mathrm{Wi}_\sigma \equiv \lambda\sigma_{\max} > 1/2$, the polymer molecule will stretch indefinitely. Figure 12 shows Wi_σ versus Wi, and Fig. 13 shows $\overline{\overline{\mathrm{tr}\,\boldsymbol{\tau}_\mathbf{p}}}$ versus Wi_σ along several experimental paths, with β =0.97 and Ex=100. The double overbar denotes volume averaging. Clearly the polymer stress becomes very large as Wi_σ passes through 1/2, and we have found no ECS to exist for which $\mathrm{Wi}_\sigma \gtrsim 0.64$. The point at El=0.019, Wi_σ=0.64 (rightmost point on the plot) is just before the ECS at that value of El loses existence (see Fig. 3).

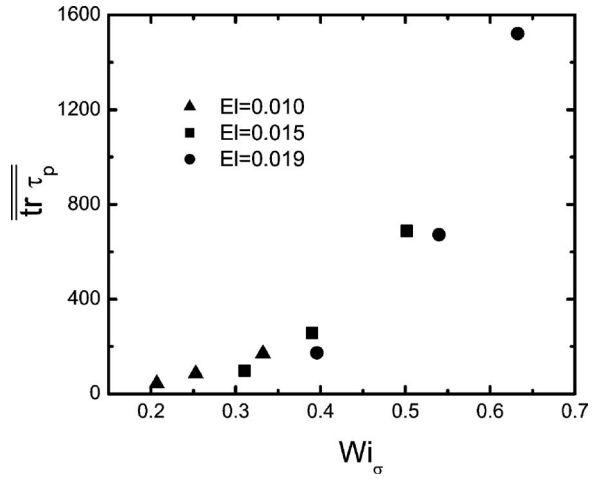

FIG. 13. Changes of polymer stress as Wi_σ increases; Ex=100, β=0.97.

B. Budgets of turbulent kinetic energy and Reynolds stress

In the plane Poiseuille ECS, the polymer becomes highly stretched in near-wall and channel centerline regions and relaxes as it moves into and around one of the streamwise vortices flanking the streak. This relaxation works to "unwind" the vortex and to reduce its strength. Since the mechanism that sustains the coherent structures depends on the vortices to regenerate the streamwise streak, the suppression of the streamwise vortices leads to a collapse of this mechanism and ultimately to drag reduction. This section looks at the budgets of turbulent kinetic energy and Reynolds stress along the experimental path of El=0.019, to better understand the changes in velocity statistics that accompany drag reduction.

The Reynolds stresses are actually $-\rho\overline{v_i' v_j'}$, but it is convenient and conventional to refer to $\overline{v_i' v_j'}$ as the Reynolds stresses, which we will do henceforth. Scaling the velocity fluctuations with u_τ and time with ν/u_τ^2, the budget equation for the Reynolds stresses for a polymer solution can be written as[51]

$$\frac{\partial \overline{v_i' v_j'}}{\partial t} + V_k \frac{\partial}{\partial x_k}\overline{v_i' v_j'} + T_{ij}^t = P_{ij} + D_{ij} + R_{ij} + T_{ij}^p + \varepsilon_{ij} + E_{ij}. \tag{13}$$

Here, the velocity, pressure, and force due to the polymer

$$\mathbf{f} = \frac{2(1-\beta)}{\mathrm{Re\,Wi}} \boldsymbol{\nabla} \cdot \boldsymbol{\tau}_p$$

are written as sums of mean and fluctuating parts ($\mathbf{v}=\mathbf{V}+\mathbf{v}'$, $p=P+p'$, and $\mathbf{f}=\mathbf{F}+\mathbf{f}'$). The first two terms of Eq. (13) are zero for the ECS since they only include x-derivatives of the averaged quantities $[(\partial/\partial t)\overline{v_i' v_j'} \to -C_v(\partial/\partial x)\overline{v_i' v_j'} = 0$ and $V_x(\partial/\partial x)\overline{v_i' v_j'} = 0]$. The terms

$$T_{ij}^t = \frac{\partial}{\partial x_k}\overline{v_i' v_j' v_k'} \tag{14}$$

and

$$T_{ij}^p = -\frac{\partial}{\partial x_k}(\overline{v_i' p'}\,\delta_{jk} + \overline{v_j' p'}\,\delta_{ik}) \tag{15}$$

are the transport of kinetic energy by the fluctuating velocities and the fluctuating pressure, respectively. The production term

$$P_{ij} = -\overline{v_i' v_k'}\frac{\partial V_j}{\partial x_k} - \overline{v_j' v_k'}\frac{\partial V_i}{\partial x_k} \tag{16}$$

generates Reynolds stresses through interaction with the mean velocity gradient. For shear flows, which have $\mathbf{V}$

$=[V_x(y),0,0]$, the terms P_{22} and P_{33} are zero. Thus, there is no production of wall-normal or spanwise velocity fluctuations due to the mean shear. The pressure-rate-of-strain term

$$R_{ij} = \overline{p'\left(\frac{\partial v_i'}{\partial x_j} + \frac{\partial v_j'}{\partial x_i}\right)}, \tag{17}$$

is traceless for an incompressible fluid and does not show up in the equation for turbulent kinetic energy, which is found by taking half the trace of Eq. (13). Therefore, this term simply redistributes energy from the streamwise velocity fluctuations to the wall-normal and spanwise velocity fluctuations. As stated earlier, there is no production of either $\overline{v_y'v_y'}$ or $\overline{v_z'v_z'}$ by the term of Eq. (16), so the terms of the pressure-rate-of-strain act as a pseudo-production term for wall-normal and spanwise velocity fluctuations. The pressure-rate-of-strain term [Eq. (17)] and the pressure transport term [Eq. (15)] are decomposition of the velocity-pressure-gradient term

$$\Pi_{ij} = R_{ij} + T_{ij}^p = -\overline{v_i'\frac{\partial p'}{\partial x_j} + v_j'\frac{\partial p'}{\partial x_i}}. \tag{18}$$

The diffusion and dissipation of Reynolds stresses are given by

$$D_{ij} = \frac{\beta}{\mathrm{Re}}\frac{\partial^2}{\partial x_k \partial x_k}\overline{v_i'v_j'} \tag{19}$$

and

$$\varepsilon_{ij} = -\frac{2\beta}{\mathrm{Re}}\overline{\frac{\partial v_i'}{\partial x_k}\frac{\partial v_j'}{\partial x_k}}, \tag{20}$$

respectively. The direct contribution of the polymer stresses to the kinetic energy budgets is the velocity-polymer-force term

$$E_{ij} = \overline{v_i'f_j' + v_j'f_i'}. \tag{21}$$

As stated earlier, the equation for turbulent kinetic energy is found by taking half the trace of Eq. (13). Figures 14–16 give the various terms in the budget of turbulent kinetic energy, $\mathrm{KE}=(\overline{v_x^2}+\overline{v_y^2}+\overline{v_z^2})/2$, for viscoelastic ECS along the experimental path of El=0.019. The maxima and minima associated with the various quantities display a pronounced monotonic decrease in amplitude with the increase of viscoelasticity. The production, diffusion, and dissipation of the turbulent kinetic energy in viscoelastic ECS are significantly reduced as Re (and Wi) increases. The transport term for the viscoelastic ECS is at a lower level in the near wall region. We also observe that near the wall, the direct contribution of the polymer increases with the increase of viscoelasticity, where the polymer stretch (and stress) is highest in the streamwise streaks. However, this polymer contribution becomes negative further away from the wall, where the streamwise velocity fluctuations increase dramatically with the increase of viscoelasticity. This observation is consistent with DNS studies.[18] It should also be noted that the scale for turbulent transport (Fig. 15) and velocity-polymer-force (Fig. 16) terms is an order smaller than the production, diffusion, and dissipation terms, while the changes in magnitude in each term due to the increases of viscoelasticity are on the same order as those changes in production, diffusion, and dissipation. In addition, a monotonic shift of maxima and minima further away from the wall is observed with the increase of viscoelasticity for each term in the kinetic energy budgets. This shift is consistent with the notion of the expansion of the elastic sublayer as has been found experimentally,[1] and all these results for the ECS mirror those found in DNS of full turbulence.[17,18]

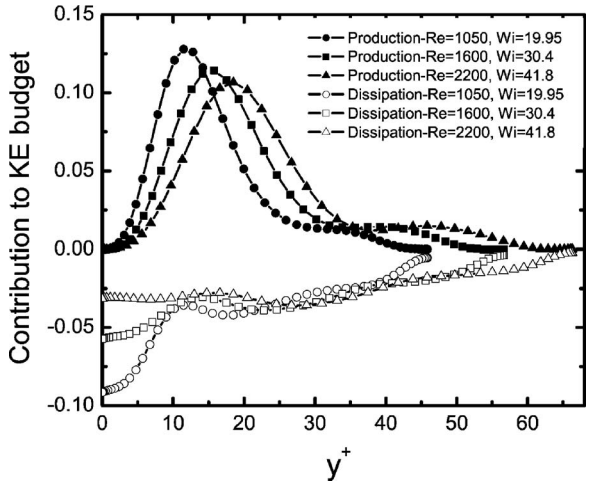

FIG. 14. The contribution to the turbulent kinetic energy budget of the production and dissipation terms for viscoelastic ECS along El=0.019, β =0.97, Ex=100.

Figures 17–19 show the contribution to the $\overline{v_x'v_y'}$ budgets along the same experimental path. The production term, which acts as a sink in this case, decreases in magnitude as Re (and Wi) increases. However, the pressure-rate-of-strain term for this budget, which acts to increase Reynolds shear stress by redistributing energy from the streamwise fluctuations, also decreases. This is again due to the polymer weakening the vortices and reducing the pressure fluctuations. The reduction in the pressure-rate-of-strain term (source) is greater than the increase in production term, especially near

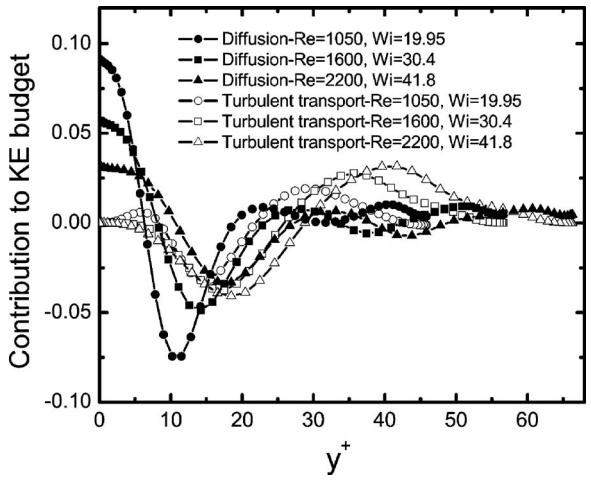

FIG. 15. The contribution to the turbulent kinetic energy budget of the diffusion and transport terms for viscoelastic ECS along El=0.019, β =0.97, Ex=100.

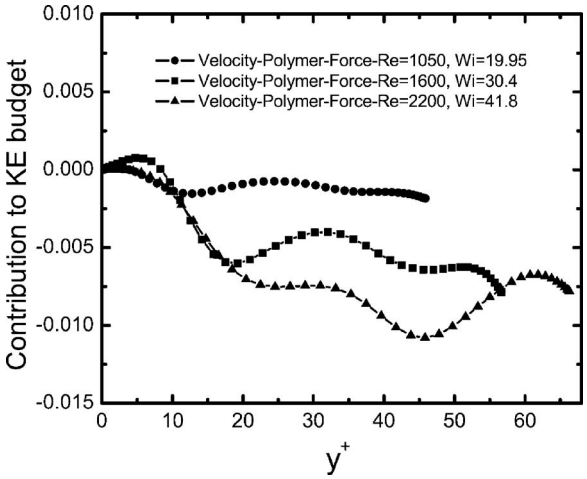

FIG. 16. The contribution to the turbulent kinetic energy budget of the velocity-polymer-force term for viscoelastic ECS along El=0.019, β=0.97, Ex=100.

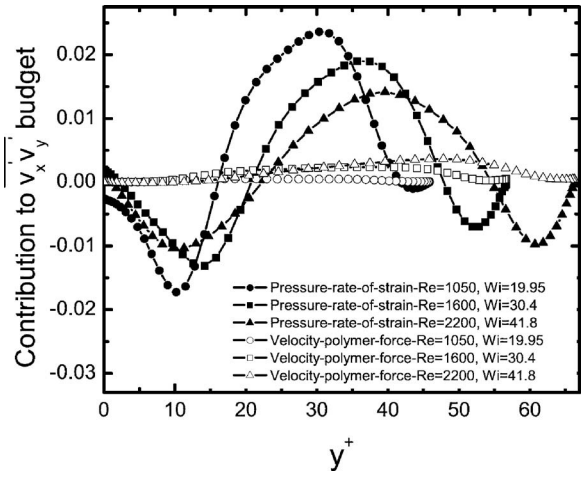

FIG. 18. The contribution to the $\overline{v_x'v_y'}$ budget of the pressure-rate-of-strain and velocity-polymer-force terms for viscoelastic ECS along El=0.019, β=0.97, Ex=100.

one quarter of the channel away from the wall, and the net effect is a decrease in the Reynolds shear stress. The velocity-pressure-gradient term (Fig. 19), which is the sum of the R_{xy} and T_{xy}^{p} terms, decreases as Re (and Wi) increases. This decrease leads to a redistribution of the turbulent kinetic energy among the streamwise and wall-normal directions, which gives rise to the enhanced rms streamwise velocity fluctuations, reduced rms wall-normal velocity fluctuations and reduced Reynolds shear stress. The velocity-polymer-force term is small in this budget because the polymer are stretched primarily in the streamwise direction (so f_y' is small) and stretching primarily occurs near the wall (so v_y' is smallest where f_x' is largest). These results closely match those found in DNS of full turbulence.[18] The agreement between our results of the $\overline{v_x'v_x'}$, $\overline{v_y'v_y'}$ budgets, and those found in DNS of fully turbulence is also very good.

It is noticed that the budgets of turbulent kinetic energy and Reynolds stress for fully turbulent flows at relatively high Reynolds number always produce a uniform region at the channel centerline, which corresponds to a homogeneous turbulent core.[17,18] This uniform region is not captured in our study due to the absence of a turbulent core, as shown in Fig. 1. However, the monotonic increase or decrease in each component of turbulent kinetic energy and Reynolds stress with the increase of viscoelasticity presented here qualitatively match those of the DNS study.[17,18] These effects of viscoelasticity on the production (and pseudo-production) terms can be attributed to the suppression of the vortices by the polymer. The effects of streamwise vortex suppression are twofold: First, the redistribution of mean shear due to the vortices is reduced, increasing the net production of streamwise velocity fluctuations by the mean shear.[51] Second, the pressure fluctuations are reduced, decreasing the transfer of energy from the streamwise velocity fluctuations to the wall-normal and spanwise directions. These results are consistent with the structural mechanism for drag reduction proposed previously.[51,54]

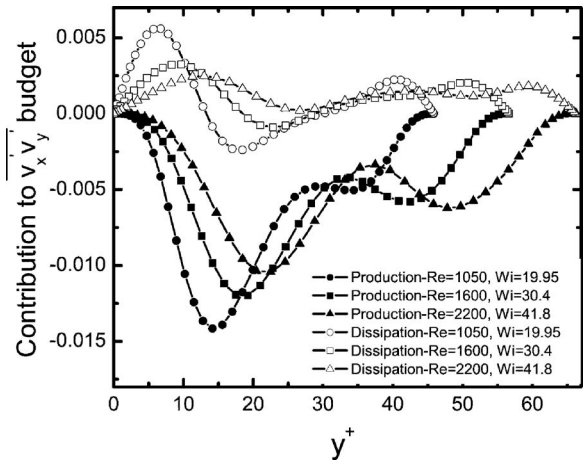

FIG. 17. The contribution to the $\overline{v_x'v_y'}$ budget of the production and dissipation terms for viscoelastic ECS along El=0.019, β=0.97, Ex=100.

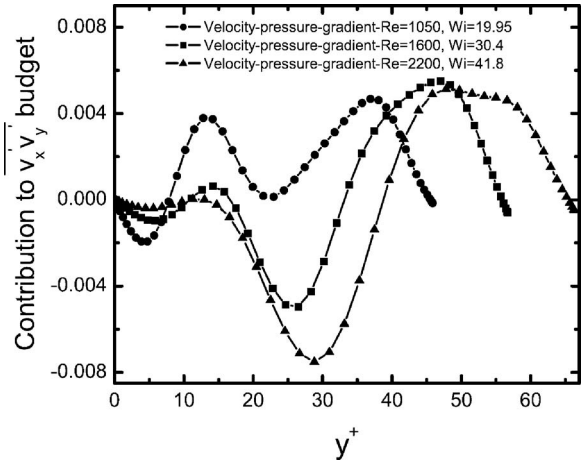

FIG. 19. The contribution to the $\overline{v_x'v_y'}$ budget of the velocity-pressure-gradient term for viscoelastic ECS along El=0.019, β=0.97, Ex=100.

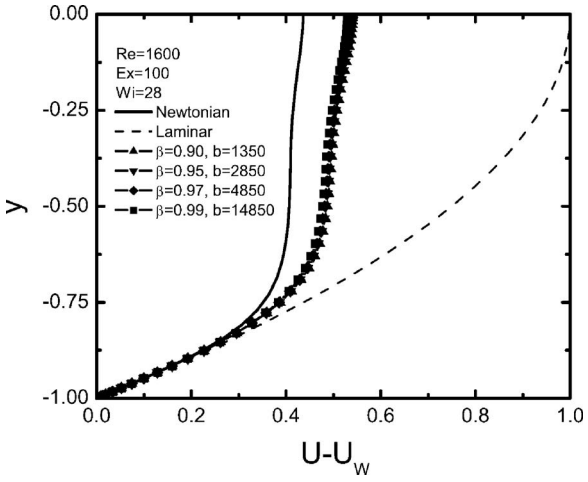

FIG. 20. Mean streamwise velocity for viscoelastic ECS; Re=1600, Ex=100, Wi=28.

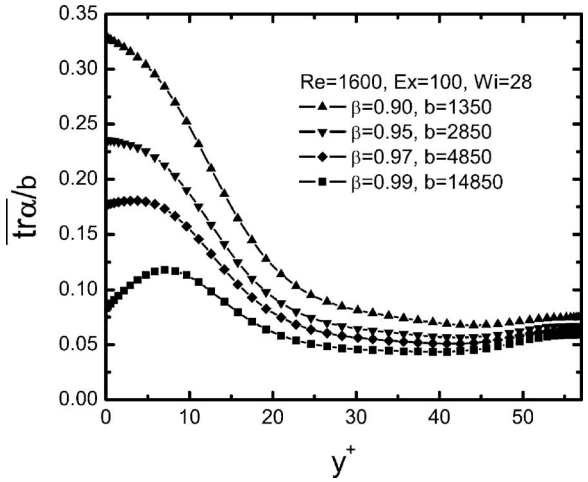

FIG. 21. Polymer stretch for viscoelastic ECS; Re=1600, Ex=100, Wi=28.

C. Effect of variation of rheological parameters

To gain more insight into the influence of rheological parameters on polymer induced drag reduction, we study the effects for different contributions of molecular extensibility b, solvent viscosity ratio β, and the extensibility parameter Ex. The comparison of our results with existing experimental and DNS studies may help us better understand the effect of polymer additives on these nonlinear traveling waves.

The extensibility parameter Ex measures the importance of the extensional polymer stress in turbulent drag reduction. Recall that for the FENE-P model, $\mathrm{Ex}=2b(1-\beta)/3\beta$. By varying β and b, it is possible to vary concentration and chain length while keeping Ex constant. Figure 20 shows the mean streamwise velocity profiles for various values of β and b, with Ex=100, Re=1600, and Wi=28. Clearly, at fixed Ex, the mean velocity is insensitive to variations of β and b. This observation indicates that the observed drag reduction effect is determined almost exclusively by the extensional viscosity and Weissenberg number for a given Re. Streamwise vorticity, rms velocity fluctuations, and Reynolds shear stress also collapse for these various polymer solutions.

Figure 21 shows the relative polymer stretch for the same conditions used for Fig. 20. With Ex=100, Re=1600, and Wi=28, polymer chains are only significantly stretched in the near-wall region due to the high wall shear rate. The relative stretch for short chain polymers is more significant than that for long chain polymers.

Since the extensibility parameter is so important, we next look at the dependence of drag reduction on Ex (it is possible to vary Ex and β while keeping b constant). The effect of Ex on the degree of drag reduction (percentage decrease in the friction factor relative to that of the Newtonian ECS at the same Re) for various polymers at Re=1600 and Wi=28 is shown in Fig. 22. Also shown (dashed line) is the maximum amount of drag reduction possible for the ECS state under the assumption that the velocity profile at the ECS existence boundary is "universal," as implied by Fig. 4. The upper limit of drag reduction within the ECS existence region at Re=1600 is about 36%. However, other types of coherent traveling wave states may be unmasked and become dominant beyond this existence region (at higher Wi for a given Re). This suggests that the maximum drag reduction (MDR) (>36% at Re=1600) is determined by the effect of viscoelasticity on these dominant structures in the MDR region. For a given polymer solution (i.e., b=const), the degree of drag reduction increases monotonically with the increase of Ex (and decrease of β), which agrees with the well-known fact that more drag reduction is observed in flows with higher extensional polymer stress. The degree of drag reduction curves for various b eventually lose existence after reaching the dashed line in Fig. 22, beyond which viscoelasticity completely suppress these nonlinear traveling waves. Another observation about Fig. 22 is that the curves for various polymers are very close in the range of Ex considered here, which again confirms our observation in Fig. 20 that the degree of drag reduction is determined almost exclusively by Ex and Wi for a given Re.

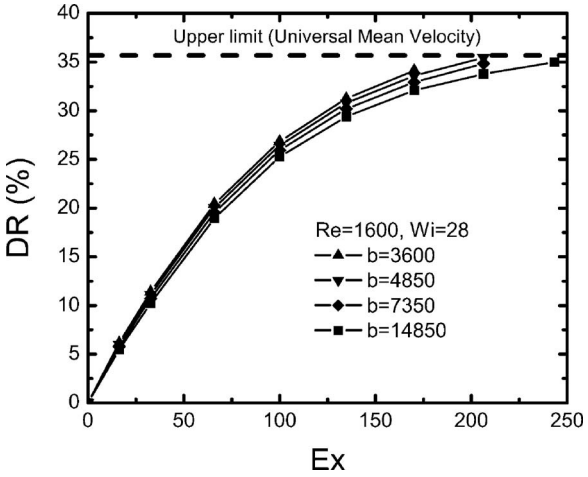

FIG. 22. Changes in drag reduction as Ex increases for viscoelastic ECS; Re=1600, Wi=28, b=3600, 4850, 7350, 14 850.

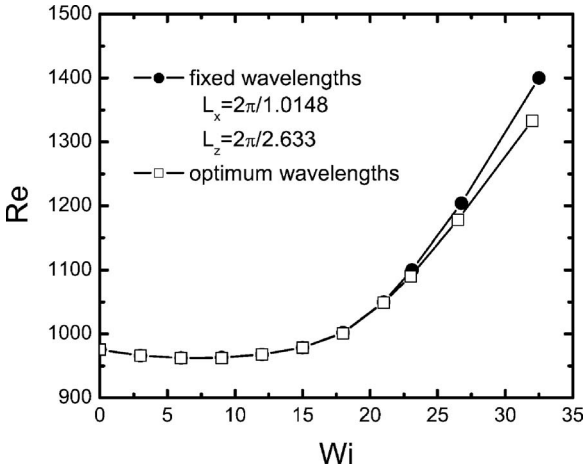

FIG. 23. Changes in the minimum Re as Wi increases with the "optimal" length scales of Newtonian and viscoelastic ECS for $\beta=0.97$, Ex=100.

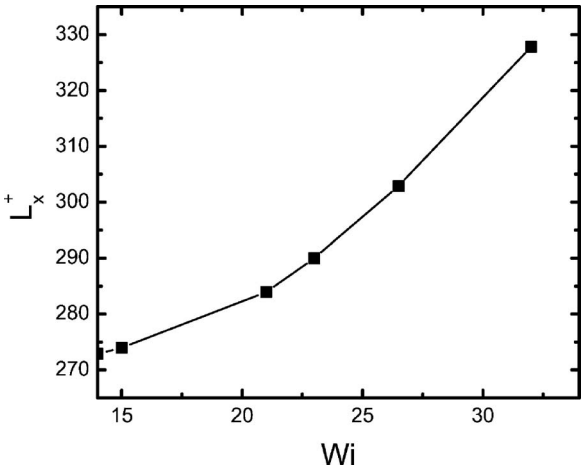

FIG. 24. Changes in optimum streamwise wavelength as Wi increases; $\beta=0.97$, Ex=100.

D. Study of optimum wavelength conditions

All results presented above are with the "optimal" length scales of Newtonian ECS. In the Newtonian limit, the minimum Reynolds number at which ECS exist is Re=977 ($\mathrm{Re}_\tau=44.2$), with $L_x=2\pi/1.0148$ and $L_z=2\pi/2.633$. In inner units, these lengths correspond at $\mathrm{Re}_\tau=44.2$ to $L_x^+=273.7$ and $L_z^+=105.5$, which quantitatively capture the length scales of streamwise vortices in the turbulent buffer layer.[9,29,39] These observations show that in Newtonian turbulence, buffer layer structure is maintained at a size in wall units that approximately corresponds to the minimum size that will support a plane Poiseuille flow ECS. We hypothesize that this principle remains valid for viscoelastic ECS. In this section, we study how the ECS existence boundary changes with these "optimal" length scales of viscoelastic ECS (i.e., the values L_x^+ and L_z^+ that lead to the smallest Re for existence of viscoelastic ECS), and how the optimal length scales of viscoelastic ECS change due to viscoelasticity.

The viscoelastic ECS solutions depend on six parameters: the streamwise wavelength L_x, the spanwise wavelength L_z, half-channel height l, the extensibility parameter Ex, the viscosity ratio β, and the Weissenberg number Wi. For a given set of Ex, β, and Wi, the minimum Re (i.e., the minimum half-channel height) at which the viscoelastic ECS first come into existence can be computed by varying L_x and L_z using the conjugate directions method, as has been used to compute the minimum Reynolds number for existence of Newtonian ECS.[29]

The ECS existence boundaries with the optimal length scales of Newtonian and viscoelastic ECS for $\beta=0.97$, and Ex=100 are shown in Fig. 23. The existence boundary with the optimal length scales of viscoelastic ECS is uniformly but slightly (no more than 5%) lower than the one with the optimal length scales of Newtonian ECS. This observation confirms the results reported recently about the viscoelastic ECS existence boundary in plane Poiseuille flow.[54] Hereafter, all the results shown are at points on the ECS existence boundary with the "optimal" length scales of viscoelastic ECS (instead of along a given experimental path).

We now turn to the study of how the streamwise, spanwise wavelengths, and wall-normal extent of ECS change with viscoelasticity. Figures 24 and 25 show the changes in streamwise and spanwise wavelengths at different Wi on the ECS existence boundary with the optimal length scales of viscoelastic ECS for $\beta=0.97$ and Ex=100. We observe that both streamwise and spanwise wavelengths increase monotonically with the increase of viscoelasticity. At Wi=32, the increases in streamwise and spanwise wavelengths are about 22% and 18%, respectively, relative to the wavelengths of Newtonian ECS at onset. These observations are consistent with experimental observations.[5,72,73] The changes in the minimum friction Reynolds number (i.e., the wall-normal extent of ECS) Re_τ, with viscoelasticity is shown in Fig. 26. With the increase of viscoelasticity, the wall-normal extent of viscoelastic ECS increases significantly. At Wi=32, the increase in the wall-normal extent of ECS is about 18%. This observation indicates that the buffer layer thickens with the increase of viscoelasticity, which is also consistent with experimental observations.[1]

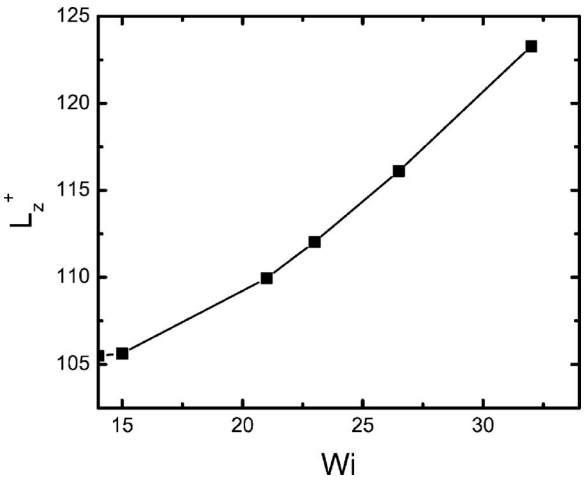

FIG. 25. Changes in optimum spanwise wavelength as Wi increases; $\beta=0.97$, Ex=100.

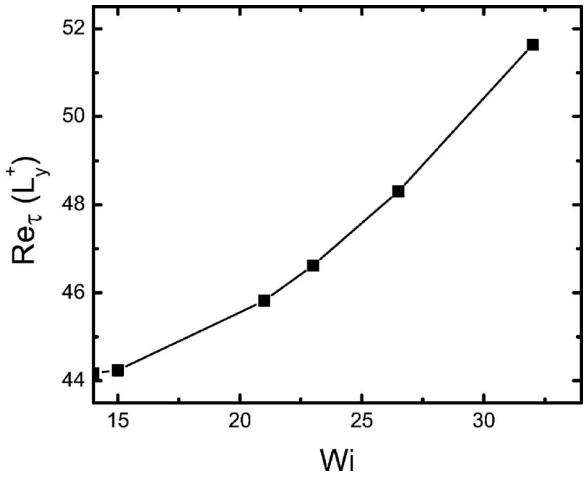

FIG. 26. Changes in wall-normal extent of ECS as Wi increases; $\beta=0.97$, Ex=100.

IV. CONCLUSIONS

The Navier-Stokes equations support nonlinear traveling wave solutions, or exact coherent states (ECS) that capture well the length scales and dominant flow structures of near-wall (buffer layer) turbulence. In this work, we have studied the effect of polymer additives on ECS in the plane Poiseuille geometry, focusing on Reynolds numbers slightly above transition. Many observations about fully turbulent flows of dilute polymer solutions at low to moderate levels of drag reduction are captured qualitatively by the effect of viscoelasticity on the channel flow ECS. Above a critical Weissenberg number, there is a dramatic increase in the minimum Reynolds number Re_{min} at which the ECS can exist. As the Reynolds number is related to the wall-normal scale of the flow structures, this result mirrors experimental observations of buffer region "thickening" in drag reducing flows. Furthermore, since evidence indicates that existence of the ECS is a prerequisite for transition to turbulence, the increase in minimum Reynolds number with increasing viscoelasticity is also consistent with the experimentally observed delay in transition to turbulence in polymer solutions. The effect of viscoelasticity on the ECS lies primarily in its influence on the streamwise vortices that sustain the flow. The polymer molecules stretch near the wall and in the upwellings between vortices, and at relatively high Wi, they relax as they enter the vortices, resisting the vortex motion, and thus reducing drag. Specifically, at sufficiently high wall shear rates, viscoelasticity completely suppresses these streamwise-aligned vortices in the near-wall region, as is found in experiments in the MDR region. These effects can also be seen in the budgets of turbulent kinetic energy, Reynolds stress, and the mean shear stress. The investigation of rheological parameters shows that the drag reduction effect is determined almost exclusively by the extensional viscosity and Weissenberg number. The study of optimum wavelengths for viscoelastic ECS shows that wavelengths in both streamwise and spanwise directions increase monotonically with the increase of drag reduction. Accompanying this observation is the thickening of ECS in wall-normal direction. All these results show that the mechanism of polymer induced drag reduction can be captured by the effect of viscoelasticity on these nonlinear traveling waves.

ACKNOWLEDGMENTS

The authors are indebted to Fabian Waleffe for many illuminating discussions and for sharing his code for computation of the Newtonian exact coherent states. This work was supported by the National Science Foundation, Grant No. CTS-0328325, and the Petroleum Research Fund, administered by the American Chemical Society.

[1] P. S. Virk, "Drag reduction fundamentals," AIChE J. **21**, 225 (1975).
[2] J. L. Lumley, "Drag reduction by additives," Annu. Rev. Fluid Mech. **1**, 367 (1969).
[3] W. D. McComb, *The Physics of Fluid Turbulence* (Oxford University Press, New York, 1990).
[4] M. D. Graham, "Drag reduction in turbulent flow of polymer solutions," in *Rheology Reviews 2004*, edited by D. M. Binding and K. Walters (British Society of Rheology, Norwich, UK, 2004), pp. 143–170.
[5] G. L. Donohue, W. G. Tiederman, and M. M. Reischman, "Flow visualization of the near-wall region in a drag-reducing channel flow," J. Fluid Mech. **50**, 559 (1972).
[6] W. G. Tiederman, T. S. Luchik, and D. G. Bogard, "Wall-layer structure and drag reduction," J. Fluid Mech. **156**, 419 (1985).
[7] D. T. Walker and W. G. Tiederman, "Turbulent structure in a channel flow with polymer injection at the wall," J. Fluid Mech. **218**, 377 (1990).
[8] M. P. Escudier, F. Presti, and S. Smith, "Drag reduction in the turbulent pipe flow of polymers," J. Non-Newtonian Fluid Mech. **81**, 197 (1999).
[9] S. K. Robinson, "Coherent motions in the turbulent boundary layer," Annu. Rev. Fluid Mech. **23**, 601 (1991).
[10] J. Jeong, F. Hussian, W. Schoppa, and J. Kim, "Coherent structures near the wall in a turbulent channel flow," J. Fluid Mech. **332**, 185 (1997).
[11] P. Holmes, J. L. Lumley, and G. Berkooz, *Turbulence, Coherent Structures, Dynamical Systems and Symmetry* (Cambridge University Press, New York, 1996).
[12] R. Sureshkumar, A. N. Beris, and R. Handler, "Direct numerical simulation of the turbulent channel flow of a polymer solution," Phys. Fluids **9**, 743 (1997).
[13] J. M. J. den Toonder, M. A. Hulsen, G. D. C. Kuiken, and F. T. M. Nieuwstadt, "Drag reduction by polymer additives in a turbulent pipe flow: numerical and laboratory experiments," J. Fluid Mech. **337**, 193 (1997).
[14] A. A. Draad, G. D. C. Kuiken, and F. T. M. Nieuwstadt, "Laminar-turbulent transition in pipe flow for Newtonian and Non-Newtonian fluids," J. Fluid Mech. **377**, 267 (1998).
[15] J. L. Lumley, "Drag reduction in turbulent flow by polymer additives," J. Polym. Sci. Macromol. Rev. **7**, 263 (1973).
[16] T. Wei and W. W. Willmarth, "Modifying turbulent structure with drag-reducing polymer additives in turbulent channel flows," J. Fluid Mech. **245**, 619 (1992).
[17] P. K. Ptasinski, B. J. Boersma, F. T. M. Nieuwstadt, M. A. Hulsen, B. H. A. A. V. D. Brule, and J. C. R. Hunt, "Turbulent channel flow near maximum drag reduction: simulations, experiments and mechanisms," J. Fluid Mech. **490**, 251 (2003).
[18] C. D. Dimitropoulos, R. Sureshkumar, A. N. Beris, and R. A. Handler, "Budgets of Reynolds stress, kinetic energy and streamwise enstrophy in viscoelastic turbulent channel flow," Phys. Fluids **13**, 1016 (2001).
[19] K. D. Housiadas and A. N. Beris, "Polymer-induced drag reduction: Effects of variations in elasticity and inertia in turbulent viscoelastic channel flow," Phys. Fluids **15**, 2369 (2003).
[20] M. D. Warholic, H. Massah, and T. J. Hanratty, "Influence of drag-reducing polymers on turbulence: effects of Reynolds number, concentration and mixing," Exp. Fluids **27**, 461 (1999).
[21] M. D. Warholic, D. K. Heist, M. Katcher, and T. J. Hanratty, "A study with particle image velocimetry of the influence of drag-reducing polymers on the structure of turbulence," Exp. Fluids **31**, 474 (2001).
[22] C. Li, R. Sureshkumar, and B. Khomami, "Influence of rheological parameters on polymer induced turbulent drag reduction," J. Non-Newtonian Fluid Mech. **140**, 23 (2006).
[23] M. Nagata, "Bifurcation in Couette flow between almost corotating cylin-

ders," J. Fluid Mech. **169**, 229 (1986).
[24]M. Nagata, "On wavy instabilities of the Taylor-vortex flow between corotating cylinders," J. Fluid Mech. **188**, 585 (1988).
[25]M. Nagata, "Three-dimensional finite amplitude solutions in plane Couette flow: bifurcation from infinity," J. Fluid Mech. **217**, 519 (1990).
[26]R. M. Clever and F. H. Busse, "Tertiary and quaternary solutions for plane Couette flow," J. Fluid Mech. **344**, 137 (1997).
[27]F. Waleffe, "Three-dimensional coherent states in plane shear flows," Phys. Rev. Lett. **81**, 4140 (1998).
[28]F. Waleffe, "Exact coherent structures in channel flow," J. Fluid Mech. **435**, 93 (2001).
[29]F. Waleffe, "Homotopy of exact coherent structures in plane shear flows," Phys. Fluids **15**, 1517 (2003).
[30]H. Faisst and B. Eckhardt, "Traveling waves in pipe flow," Phys. Rev. Lett. **91**, 224502 (2003).
[31]H. Wedin and R. R. Kerswell, "Exact coherent structures in pipe flow: travelling wave solutions," J. Fluid Mech. **508**, 333 (2004).
[32]J. Jeong and F. Hussain, "On the identification of a vortex," J. Fluid Mech. **285**, 69 (1995).
[33]Y. Dubief and F. Delcayre, "On coherent-vortex identification in turbulence," J. Turbul. **1**, 1 (2000).
[34]J. Z. Wu, A. K. Xiong, and Y. T. Yang, "Axial stretching and vortex definition," Phys. Fluids **17**, 038108 (2005).
[35]F. Waleffe and J. Wang, "R^{-1} scaling of lower branch exact coherent structures," in *IUTAM Symposium on Laminar-Turbulent Transition and Finite Amplitude Solutions* (Springer, Dordrecht, 2005), pp. 85–106.
[36]S. Bottin, O. Dauchot, F. Daviaud, and P. Manneville, "Experimental evidence of streamwise vorticities as finite amplitude solutions in transitional plane Couette flow," Phys. Fluids **10**, 2597 (1998).
[37]R. B. Bird, W. E. Stewart, and E. N. Lightfoot, *Transport Phenomena*, 2nd ed. (Wiley, New York, 2002).
[38]D. R. Carlson, S. E. Widnall, and M. F. Peeters, "A flow-visualization study of transition in plane Poiseuille flow," J. Fluid Mech. **121**, 487 (1982).
[39]J. Jiménez and P. Moin, "The minimal flow unit in near wall turbulence," J. Fluid Mech. **225**, 221 (1991).
[40]S. B. Pope, *Turbulent Flows* (Cambridge University Press, New York, 2000).
[41]P. A. Stone, "Viscoelastic exact coherent states in plane shear flows," Ph.D. thesis, University of Wisconsin-Madison, 2004.
[42]S. H. Strogatz, *Nonlinear Dynamics and Chaos: With Applications to Physics, Biology, Chemistry and Engineering* (Addison Wesley, New York, 1994).
[43]G. Kawahara and S. Kida, "Periodic motion embedded in plane Couette turbulence: regeneration cycle and burst," J. Fluid Mech. **449**, 291 (2001).
[44]S. Toh and T. Itano, "A periodic-like solution in channel flow," J. Fluid Mech. **481**, 67 (2003).
[45]J. Jiménez and M. P. Simens, "Low-dimensional dynamics of a turbulent wall flow," J. Fluid Mech. **435**, 81 (2001).
[46]J. M. Hamilton, J. Kim, and F. Waleffe, "Regeneration mechanisms of near-wall turbulent structures," J. Fluid Mech. **287**, 317 (1995).
[47]F. Waleffe, "On a self-sustaining process in shear flows," Phys. Fluids **9**, 883 (1997).
[48]P. G. Drazin and W. H. Reid, *Hydrodynamic Stability* (Cambridge University Press, New York, 1981).
[49]P. A. Stone, F. Waleffe, and M. D. Graham, "Toward a structural understanding of turbulent drag reduction: nonlinear coherent states in viscoelastic shear flows," Phys. Rev. Lett. **89**, 208301 (2002).
[50]P. A. Stone and M. D. Graham, "Polymer dynamics in a model of the turbulent buffer layer," Phys. Fluids **15**, 1247 (2003).
[51]P. A. Stone, A. Roy, R. G. Larson, F. Waleffe, and M. D. Graham, "Polymer drag reduction in exact coherent structures of plane shear flow," Phys. Fluids **16**, 3470 (2004).
[52]W. Li, P. A. Stone, and M. D. Graham, "Viscoelastic nonlinear traveling waves and drag reduction in plane Poiseuille flow," in *IUTAM Symposium on Laminar-Turbulent Transition and Finite Amplitude Solutions* (Springer, Dordrecht, 2005), pp. 285–308.
[53]Y. Dubief, C. M. White, V. E. Terrapon, E. Shaqfeh, P. Moin, and S. K. Lele, "On the coherent drag-reducing and turbulence-enhancing behaviour of polymers in wall flows," J. Fluid Mech. **514**, 271 (2004).
[54]W. Li, L. Xi, and M. D. Graham, "Nonlinear travelling waves as a framework for understanding turbulent drag reduction," J. Fluid Mech. **565**, 353 (2006).
[55]R. B. Bird, C. F. Curtiss, R. C. Armstrong, and O. Hassager, *Dynamics of Polymeric Liquids*, 2nd ed. (Wiley, New York, 1987), Vol. 2.
[56]S. K. Lele, "Compact finite difference schemes with spectral-like resolution," J. Comput. Phys. **103**, 16 (1992).
[57]T. Min, J. Y. Yoo, and H. Choi, "Effect of spatial discretization schemes on numerical solution of viscoelastic fluid flows," J. Non-Newtonian Fluid Mech. **100**, 27 (2001).
[58]R. Sureshkumar and A. N. Beris, "Effect of artificial stress diffusivity on the stability of numerical calculations and the flow dynamics of time-dependent viscoelastic flows," J. Non-Newtonian Fluid Mech. **60**, 53 (1995).
[59]S. Sibilla and A. Baron, "Polymer stress statistics in the near-wall turbulent flow of a drag-reducing solution," Phys. Fluids **14**, 1123 (2002).
[60]W. B. Giles and W. T. Pettit, "Stability of dilute viscoelastic flows," Nature (London) **216**, 470 (1967).
[61]W. D. White and D. M. McEligot, "Transition of mixtures of polymers in a dilute aqueous solution," J. Basic Eng. **92**, 411 (1970).
[62]T. Min, J. Y. Yoo, H. Choi, and D. D. Joseph, "Drag reduction by polymer additives in a turbulent channel flow," J. Fluid Mech. **486**, 213 (2003).
[63]T. Wei and W. W. Willmarth, "Reynolds-number effects on the structure of a turbulent channel flow," J. Fluid Mech. **204**, 57 (1989).
[64]J. Kim, P. Moin, and R. Moser, "Turbulence statistics in fully developed channel flow at low Reynolds number," J. Fluid Mech. **177**, 133 (1987).
[65]E. De Angelis, C. M. Casciola, and R. Piva, "DNS of wall turbulence: dilute polymers and self-sustaining mechanisms," Comput. Fluids **31**, 495 (2002).
[66]R. Seydel, *Practical Bifurcation and Stability Analysis: From Equilibrium to Chaos* (Springer-Verlag, New York, 1994).
[67]A. J. Lichtenberg and M. A. Lieberman, *Regular and Chaotic Dynamics*, 2nd ed. (Springer-Verlag, New York, 1992).
[68]J. L. Lumley, "On the solution of equations describing small scale deformation," Symp. Math. **9**, 315 (1972).
[69]E. Balkovsky, A. Fouxon, and V. Lebedev, "Turbulent dynamics of polymer solutions," Phys. Rev. Lett. **84**, 4765 (2000).
[70]E. Balkovsky, A. Fouxon, and V. Lebedev, "Turbulence of polymer solutions," Phys. Rev. E **64**, 056301 (2001).
[71]M. Chertkov, "Polymer stretching by turbulence," Phys. Rev. Lett. **84**, 4761 (2000).
[72]C. M. White, V. S. R. Somandepalli, and M. G. Mungal, "The turbulence structure of drag-reduced boundary layer flow," Exp. Fluids **36**, 62 (2004).
[73]D. K. Oldaker and W. G. Tiederman, "Spatial structure of the viscous sublayer in drag reducing channel flows," Phys. Fluids **20**, S133 (1977).